Available online at www.sciencedirect.com
ScienceDirect
Journal of Hazardous Materials 152 (2008) 493–505
Journal of Hazardous Materials
www.elsevier.com/locate/jhazmat

Experimental and numerical study of heavy gas dispersion in a ventilated room

Laurent Ricciardi *, Corinne Prévost, Laurent Bouilloux, Roger Sestier-Carlin

Institute for Radiological Protection and Nuclear Safety (IRSN), Airborne Pollutants and Containment Study and Research Department, DSU/SERAC, BP 68, 91192 Gif-sur-Yvette cedex, France

Received 5 April 2007; received in revised form 3 July 2007; accepted 4 July 2007
Available online 17 July 2007

Abstract

In order to better evaluate the consequences of an accidental release of heavy gas, such as uranium hexafluoride (UF_6), in some installations in the nuclear fuel cycle, an experimental and numerical study was conducted by IRSN on heavy gas dispersion in a ventilated room. This study was based on about 20 injection configurations of a large quantity of a heavy tracer gas, sulphur hexafluoride (SF_6), inside two ventilated rooms of different sizes. Stratification of the tracer gas was detected in all the configurations studied, even at low concentrations. Numerical simulations performed with the multidimensional CFX code enabled the stratification and the concentration levels reached in the rooms to be predicted overall, and the higher the air flow rate, the more satisfactory the comparison between simulation and experiment.

Keywords: Dispersion; Heavy gas; SF6; Gas tracing; CFD simulation

1. Introduction

As part of the analysis of On-site Emergency Plans developed by the operators of basic nuclear installations, IRSN has responsibility particularly for evaluating chosen accident scenarios and their consequences for the environment. Some facilities in the fuel cycle use uranium hexafluoride (UF_6), the behaviour of which in the event of an accidental release into a ventilated room needs to be studied in more detail to provide a more realistic evaluation of the consequences for the environment. To do that, a research programme to study the accidental release of UF_6 was conducted in collaboration with AREVA NC, EURODIF and FBFC. One of the steps in this programme was to study the behaviour of a heavy gas in a ventilated room. Indeed, because of its high density (12), UF_6 emitted as a gas is strongly affected by gravity, which largely determines the quantities involved in the process of hydrolysis with the ambient humidity. Because the products of this reaction are particularly harmful (HF and UO_2F_2 aerosols), evaluating their release into the room, and subsequently into the environment (mainly via the stack after transfer to the ventilation system) is essential. A study was therefore conducted to characterize the dispersion of a heavy tracer gas in rooms of different sizes. This study was based partly on a broad programme of experiments to study the dispersion of sulphur hexafluoride (SF_6, with a density of 5) and partly on multidimensional simulations of all the tests. The final aim was to evaluate the ability of the chosen computation code (CFX) to predict satisfactorily the dispersion behaviour of a heavy gas, with a view to its subsequent application to the study of scenarios involving UF_6 gas release.

2. Description of the experimental programme

2.1. Study parameters

The experimental programme was based entirely on the use of tracer gas techniques [1,2], the value of which lies in the use of a substance that simulates the behaviour of the gas being studied (in terms of dispersion), for which both production and specific analysis are controlled. In our case, the chosen tracer gas was sulphur hexafluoride (SF_6). The programme was constructed on the basis of interpretations of data for accident scenarios, in terms of gas concentrations and air exchange rates in the rooms. From these, it was determined that UF_6 leaks lasting

* Corresponding author. Tel.: +33 1 69 08 44 15; fax: +33 1 69 08 36 80.
E-mail address: laurent.ricciardi@irsn.fr (L. Ricciardi).

0304-3894/$ – see front matter © 2007 Elsevier B.V. All rights reserved.
doi:10.1016/j.jhazmat.2007.07.034

Nomenclature

C_{max}	maximum tracer concentration (ppm-vol)
$C_{\varepsilon 1}$	k–ε turbulence model unitless constant equal to 1.44
$C_{\varepsilon 2}$	k–ε turbulence model unitless constant equal to 1.92
$C_{\varepsilon 3}$	k–ε turbulence model unitless constant equal to 1.0
C_μ	k–ε turbulence model unitless constant equal to 0.09
D_h	hydraulic diameter (m)
D_{inj}	injection diameter (m)
Fr	Froude number
g	gravitational acceleration vector (m s^{-2})
G_k	buoyancy production rate of turbulence due to mean density gradients (kg m^{-1} s^{-3})
H	jet height (m)
k	turbulence kinetic energy per unit mass (m^2 s^{-2})
M	molar mass of gaseous mixing (kg mol^{-1})
M_{air}	molar mass of air equal to 29 g mol^{-1}
M_{SF_6}	molar mass of SF_6 equal to 146 g mol^{-1}
P	static (thermodynamic) pressure (kg m^{-1} s^{-2})
P'	modified pressure (kg m^{-1} s^{-2})
P_k	production rate of turbulence due to mean velocity gradients (kg m^{-1} s^{-3})
q_{inj}	injection flow rate of SF_6 (m^3 s^{-1})
Q	airflow rate (m^3 s^{-1})
r	ideal gas law constant equal to 8.314 J kg^{-1} mol^{-1}
R	air exchange rate (h^{-1})
t	time (s)
t_{inj}	injection duration of SF_6 (s)
T	gaseous mixing temperature equal to 293 K
Tr	transpose of matrix
u_{in}	inlet velocity (m s^{-1})
U	velocity vector (m s^{-1})
V_{inj}	injection velocity of SF_6 (m s^{-1})
X	jet range (m)
Y_{SF_6}	mass fraction of SF_6 (dimensionless)
Z	room height (m)

Greek letters

ε	turbulence Eddy dissipation rate (m^2 s^{-3})
μ	molecular (dynamic) viscosity (kg m^{-1} s^{-1})
μ_{eff}	effective viscosity (kg m^{-1} s^{-1})
μ_t	turbulence dynamic viscosity – eddy viscosity (kg m^{-1} s^{-1})
ν_t	turbulence kinematic viscosity – eddy diffusivity (m^2 s^{-1})
ρ	gaseous mixing density (kg m^{-3})
ρ_a	ambient density (kg m^{-3})
ρ_{inj}	injection density (kg m^{-3})
σ_k	dimensionless turbulence model constant for the k equation equal to 1.0
$\sigma_{k\varepsilon}$	dimensionless constant in the k–ε turbulence model equal to 1.3
σ_t	dimensionless Schmidt number equal to 1.0
τ	air exchange time (s)
Γ	dynamic diffusivity of SF_6 (kg m^{-1} s^{-1})

less than 15 min would lead to gas concentrations of between 10^4 and 10^5 ppm-vol. In addition, the volume of the rooms in which accidental gas releases could occur was between 1000 and 48,000 m^3 and the air exchange rate was between 0.2 and 3 h^{-1}. Fixed parameter values, such as the ventilation rates and modes of operation and the tracer injection flow rates and durations, were chosen on the basis of all these data, taking account of the theoretical maximum pollutant concentrations to be reached. The maximum concentration theoretically reached at injection time t_{inj} at all points in a room with uniform air exchange rate R (i.e. $1/\tau$, with τ the air exchange time) is given by the following expression [1,2]:

$$C_{max} = \frac{q_{inj}}{Q}\left(1 - \exp\left(-\frac{t_{inj}}{\tau}\right)\right) \quad (2.1)$$

It should be noted that the above expression is based on the assumption of a uniform pollutant concentration in the room. In the present study, the release of a heavy gas leads to a gas stratification in the room. Hence, this expression is only used for evaluating the theoretical mean gas concentration by the end of injection.

In each of the tests, the main results studied were the homogeneity of air exchange in the room and the space–time evolution of the concentrations and transfer kinetics at different points on three planes at different heights. The experiment rooms (Fig. 1 and Fig. 2), at the IRSN/Saclay site, were of different volumes (36 m^3 and 1500 m^3), so the range of actual concentrations could be covered while producing reasonable quantities of tracer.

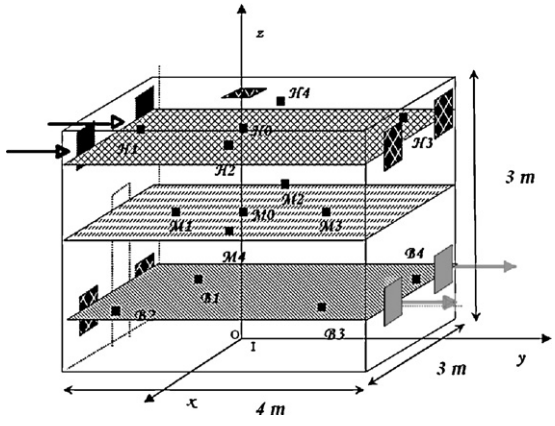

Fig. 1. Description of the mapping of sampling points in the 36 m^3 room; the heights of the lower/middle/upper planes are 0.55 m/1.5 m/2.5 m, respectively.

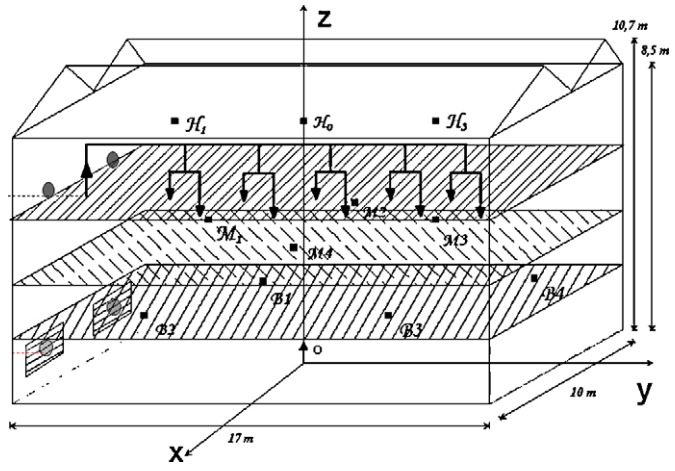

Fig. 2. Description of the mapping of the sampling points in the 1500 m^3 room; the heights of the lower/middle/upper planes are 2 m/4 m/7 m, respectively.

2.2. Construction of the test grids

The test grids (Tables 1 and 2) produced in turn in the two rooms were developed on the basis of the choices described above; the maximum theoretical concentrations of tracer evolved as a result from 10^3 to 3×10^4 ppm-vol, for injection durations 't_{inj}' from 2 to 15 min.

The air exchange rates 'R' were uniform at between 0.2 and 3 h^{-1}. In addition, because of the scenarios, the injection velocities 'V_{inj}' of the tracer gas were between 6 and 42 m s^{-1} (the injection diameters 'D_{inj}' were adapted to the injected flow rates). The injection nozzles were set vertically, pointing upwards, for all the configurations tested. In order to characterize the stratified turbulent flow regime, the Froude, Richardson and Reynolds numbers at injection have been added in Tables 1 and 2 for each test.

Finally, two ventilation operation modes for the rooms were studied: continuous and discontinuous. In discontinuous mode

Table 1
Test grid for the 36 m^3 room

Air exchange rate (R) (h^{-1})	Test number	Emission rate (V_{inj}) (m s^{-1})	Emission time (t_{inj}) (min)	Emission tube diameter (D_{inj}) (mm)	Jet Froude number	Jet Richardson number	Jet Reynolds number
1	1	13	2	5	4,307	2.32×10^{-4}	27,857
	2	6	15	3	1,529	6.54×10^{-4}	7,714
	3	42	2	12	18,731	5.34×10^{-5}	216,000
	4	22	15	5	12,334	8.11×10^{-5}	47,143
3	5	14	2	5	4,995	2.00×10^{-4}	30,000
	6	8.5	15	3	3,069	3.26×10^{-4}	10,929
	7	20	2	12	4,247	2.35×10^{-4}	102,857
	8	30	15	5	22,936	4.36×10^{-5}	64,286
	9	9	15	12	860	1.16×10^{-3}	46,286
[2 × 3′; 0,4 × 4′; 0.8][a]	10	19	5	3	15,333	6.52×10^{-5}	24,429
[2 × 3′; 0,4 × 15′; 0.8]	11	19	5	3	15,333	6.52×10^{-5}	24,429
[2 × 3′; 0,4 × 4′; 0.8]	12	11	5	12	1,285	7.78×10^{-4}	56,571
[3.5 × 0.5′; 0,4 × 4′; 0.8]	13	8.5	15	3	3,069	3.26×10^{-4}	10,929
	15	35	15	5	31,218	3.20×10^{-5}	75,000

[a] In this case for example, the tests were produced in the discontinuous ventilation mode corresponding to (R set at 2 h^{-1} for 3 min, then R set at 0.4 h^{-1} for 4 min and finally R reduced to 0.8 h^{-1}).

Table 2
Test grid for the 1500 m^3 room

Air exchange rate (R) (h^{-1})	Test number[b]	Emission rate (V_{inj}) (m s^{-1})	Emission time (t_{inj}) (min)	Emission tube diameter (D_{inj}) (mm)	Jet Froude number	Jet Richardson number	Jet Reynolds number
0.3	16BH	13	15	12	1,795	5.57×10^{-4}	66,857
0.2	16B	15			2,389	4.19×10^{-4}	77,143
1.2	17	16			2,718	3.68×10^{-4}	82,286
3	18B	23			5,617	1.78×10^{-4}	118,286
	18H	22			5,139	1.95×10^{-4}	113,143
[2 × 3′; 0 × 15′; 0.2][a]	19B	19			3,833	2.61×10^{-4}	97,714
	19H	17			3,069	3.26×10^{-4}	87,429

[a] In this case, the tests were produced in the discontinuous ventilation mode corresponding to (R set at 2 h^{-1} for 3 min, then R set at 0 h^{-1} for 15 min and finally R reduced to 0.2 h^{-1}).

[b] BH means that the test was performed with the ventilation configuration 'Low and High Exhaust' simultaneously; H means that the test was performed with 'High Exhaust' and B means that it was performed with 'Low Exhaust'.

Table 3
Coordinates of the measurement points and the ventilation openings for the 36 m^3 room

Location	Coordinates (x, y, z) (m)	Location	Coordinates (x, y, z) (m)	Location	Coordinates (x, y, z) (m)
B1	(−1, −1, +0.55)	M0	(0, 0, +1.5)	H0	(0, 0, +2.5)
B2	(+1, −1.5, +0.55)	M1	(0, −1, +1.5)	H1	(0, −1.5, +2.5)
B3	(+1, +1, +0.55)	M2	(−1, 0, +1.5)	H2	(+1, 0, +2.5)
B4	(−1, +1.5, +0.55)	M3	(0, +1, +1.5)	H3	(0, +1.5, +2.5)
		M4	(+1, 0, +1.5)	H4	(−1, 0, +2.5)
Exhaust opening 1	(−1, +2, +0.55)			Blowing opening 1	(−1, −2, +2.5)
Exhaust opening 2	(+1, +2, +0.55)			Blowing opening 2	(+1, −2, +2.5)

(tests 10 to 13, 15, 19B and 19H), the nominal ventilation of the room operated at a fixed air exchange rate, and was then stopped for a short period before being restarted in a reduced service mode known as 'purification' mode, which provided a low air exchange rate. For each of the configurations tested, continuous monitoring of the time evolution in SF_6 concentrations at the different measurement points (Figs. 1 and 2, Tables 3 and 4) was performed using special gas analysers operating on the principle of infrared absorption of the SF_6 (Emerson Binos E devices). These analysers offer continuous real-time detection of large ranges of gas concentrations (from a few ppm-vol to several percent).

2.3. Description of the injection and sampling points

For each of the rooms and configurations tested, the injection point I of the tracer was always situated in the middle of the room, at a height of 0.15 m. Below this point I, on the floor, is located the source point O in the orthonormal reference system used for the precise positioning of all the sampling points. In all cases, there were between 11 and 14 tracer gas sampling points distributed evenly throughout the lower, middle and upper planes in the rooms tested (Figs. 1 and 2).

The 'High Blowing and Low Exhaust' ventilation configuration was fixed for all the tests carried out in the 36 m^3 room; so two blowing openings and two exhaust openings (0.15 m width × 0.1 m height) were operational. The velocities induced by the blowing, taking account of the flow rates used, therefore lay between 0.3 and 1.1 m s^{-1}.

The ventilation configurations 'Middle Blowing and Low Exhaust' then 'Middle Blowing and High Exhaust' were tested in turn during the tests conducted in the 1500 m^3 room; thus, the 10 blowing openings (distributed into 5 separate modules) arranged along the length of the room, and the two low and high exhaust openings (0.31 m diameter) were activated. The velocities induced per blowing opening, taking account of the flow rates used in turn, lay therefore between 0.15 and 1.7 m s^{-1}.

It should be noted that all the tracer sampling points located in each room could not be used during an experimental test, due to the limitation of the number of available measuring channels (four analysers comprising two channels) and to the levels of concentration to be measured in each point. Therefore, for each experimental configuration described (called "test *n*"), at least two series of tests were necessary in order to cover all the measurement points within each of the rooms. In addition, to evaluate the reproducibility of the results, each of these series was reproduced at least once, except in the exceptional case where the quantities of gas injected were too high. Therefore, at least four tests were performed for each experimental configuration studied.

Finally, once all the parameters for SF_6 gas injection (injection flow rate and duration) and ventilation of the room (air exchange rate) were well controlled, there was good reproducibility of the test results. In addition, we estimated the accuracy of the injection (mass flow rate of the tracer gas) and detection (BINOS system) devices at around 10% on the concentration values.

2.4. Principal findings of the experimental study

It should be noted that only a few examples of the results of the experiments are presented here to illustrate our remarks, but that most of the test results were then compared directly with the results of the simulation (see paragraph 3).

Table 4
Coordinates of the measurement points and the ventilation openings for the 1500 m^3 room

Location	Coordinates (x, y, z) (m)	Location	Coordinates (x, y, z) (m)	Location	Coordinates (x, y, z) (m)
B1	(−2.5, −4, +2)	M1	(0, −4, +4)	H0	(0, 0, +7)
B2	(+2.5,−6, +2)	M2	(−2, 0, +4)	H1	(0, −4, +7)
B3	(+2.5, +4, +2)	M3	(0, +4, +4)	H3	(0, +4, +7)
B4	(−2.5, +6, +2)	M4	(+2, 0, +4)		
Low Exhaust opening 1	(−2, −8.5, +0.6)	Blowing opening 1	(0, −7.1, +5)	Blowing opening 6	(0, +0.7, +4)
Low Exhaust opening 2	(+2, −8.5, +0.6)	Blowing opening 2	(0, −5.7, +4)	Blowing opening 7	(0, +2.5, +5)
High exhaust opening 1	(−2, −8.5, +5.5)	Blowing opening 3	(0, −3.9, +5)	Blowing opening 8	(0, +3.9, +4)
High exhaust opening 2	(+2, −8.5, +5.5)	Blowing opening 4	(0, −2.5, +4)	Blowing opening 9	(0, +5.7, +5)
		Blowing opening 5	(0, −0.7, +5)	Blowing opening 10	(0, +7.1, +4)

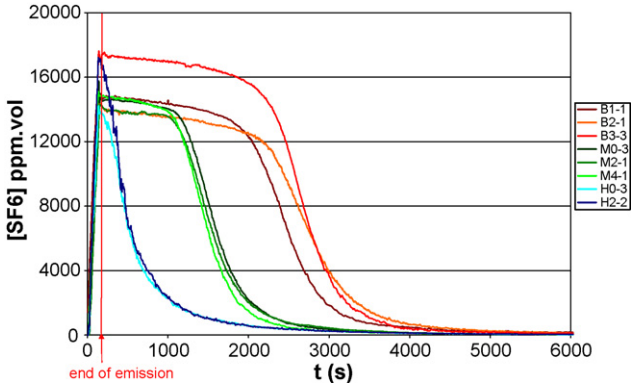

Fig. 3. Summary of results with test 3 (high injection velocity).

In many of the configurations tested, stratification of the injected gas was observed throughout the room, with accentuated gas accumulation on the floor from the start of injection, continuing until the end of injection.

These effects had already been identified in the preliminary tests for the study aimed at characterizing the dispersion of gas injected continuously but with a strong dilution (100 ppm-vol): the gas tended to accumulate on the ground throughout injection.

Overall, the time evolution of the gas concentration at points located on the lower plane was most often dependent on the gas injection dynamic; there was greater dispersion of the gas throughout the rest of the room, particularly in the smaller room, when the injection velocity was high (test 3 example, Fig. 3). We noted in test 3 carried out in the 36 m^3 room that the gas concentration levels reached at the end of injection were the same at all points because of the high injection velocity of the gas.

The ventilation effect on dispersion was more marked in the larger room, where the range of the injection nozzle was smaller.

It was also observed that operating the ventilation in discontinuous mode did not have a significant effect on stratification (Fig. 4); a slower decrease in concentrations at the low points was observed only in configuration 11, where the ventilation was stopped for a longer time (15 min) than in configuration 10 (4 min).

Finally, it was noted that, in many cases, the maximum concentration was reached after the injection of SF_6 had finished (some seconds or even minutes after), particularly at points situated on the middle and upper planes of the room: in these cases, the time evolutions of concentration were linked to the exchange of matter between zones as a result of the turbulent diffusion of the flow.

2.5. Note

In view of the difficulty reading graphs of the time evolution of the gas concentration at all the sampling points, a simplified representation of the results (monitoring of the concentration at a single point on the Bottom, Middle and High plane) was adopted for the rest of this publication. Besides, in order to improve the comparison between CFX predictions and experimental data (Figs. 14–17), the mean concentration and the associated standard deviation at each measurement plane were added to the single point concentration evolution.

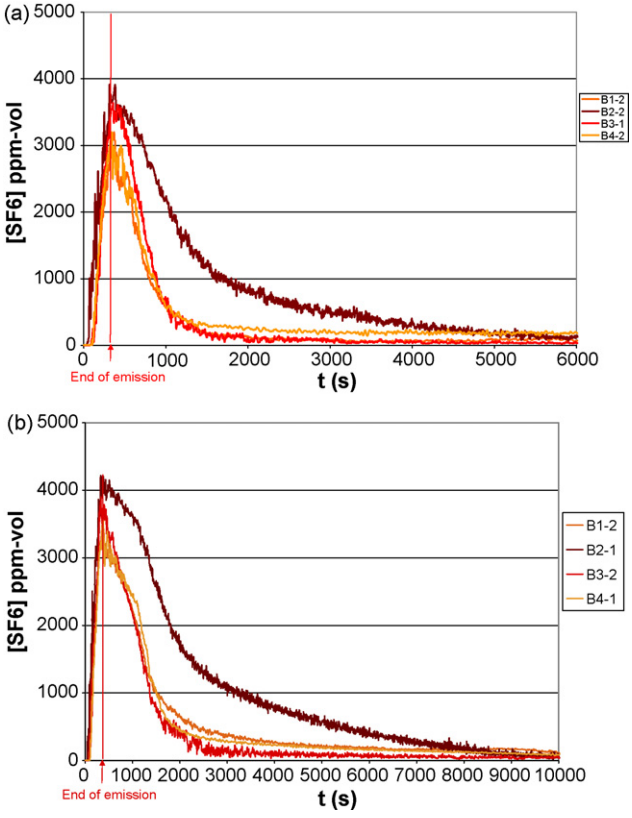

Fig. 4. Summary of results in the tests 10 (a) and 11 (b) at low plane.

3. Description of the multidimensional simulations

3.1. Introduction

All the SF_6 dispersion simulations in a ventilated room were performed using the computation code CFX-5 (version 5.5.1). As for most of the CFD codes, the governing partial differential equations are integrated over control volumes and the integral equations are converted to a system of algebraic equations. CFX-5 uses a single cell, unstaggered, collocated grid to overcome the decoupling of pressure and/or velocity, and uses a coupled solver, in which all the hydrodynamic equations are solved as a single system. This coupled solver is faster than the traditional segregated solver (such as SIMPLE) and fewer iterations are required to obtain a converged flow solution. More details can be found in the user manual of the code [4], or in [6], where is summarized the description of the main components of this CFD code (mesh system, solver and post processing) and the numerical methods used.

3.2. Equations

The equations solved in the computations performed are based on the following hypotheses. The fluid under consideration is a mixture of air and SF_6, and it is assumed that these

two components are mixed at a molecular level (multispecies formulation). The flow was assumed to be turbulent, isothermal (20 °C) and weakly compressible. The gaseous mixture, meanwhile, was assumed to be thermodynamically perfect. In addition, before any injection of SF_6, airflow was assumed to be stationary. So the computation was carried out in three stages: steady state computation of the flow in the room, transient computation of the SF_6 injection phase (2 or 15 min depending on the test) and transient computation of the decrease in concentrations once injection had stopped.

The mean flow was governed by the Navier-Stokes equations using the traditional approach known as RANS (Reynolds Averaged Navier Stokes). The SF_6 mass fraction was described by a transport equation in which the molecular diffusion coefficient and the turbulent diffusion coefficient feature, the latter being dominant in most of the flow. The turbulence correlations (Reynolds stresses and turbulent fluxes) were modelled by introducing the concept of turbulence viscosity μ_t, calculated using the classic standard k–ε first-order turbulence model. This approach was also chosen for the study of heavy (or light) gas dispersion in the environment [6–9]. Other turbulence models (particularly second-order models) were tested during the study, without any notable change in the results (see Section 3.4). Finally, the density of the gaseous mixture was given by the ideal gas law.

So the equations were as follows:

Continuity equation:

$$\frac{\partial \rho}{\partial t} + \nabla \cdot (\rho U) = 0 \tag{3.1}$$

Momentum equation:

$$\frac{\partial (\rho U)}{\partial t} + \nabla \cdot (\rho U \otimes U) = -\nabla P' + \nabla \cdot \left[(\mu + \mu_t)(\nabla U + (\nabla U)^{\mathrm{Tr}})\right] + \rho g \tag{3.2}$$

SF_6 transport equation:

$$\frac{\partial}{\partial t}(\rho Y_{SF_6}) + \nabla \cdot (\rho U Y_{SF_6}) = \nabla \cdot \left[(\Gamma + \frac{\mu_t}{\sigma_t})\nabla Y_{SF_6}\right] \tag{3.3}$$

Ideal gas law:

$$\rho = \frac{PM}{rT} \tag{3.4}$$

with

$$\frac{1}{M} = \frac{Y_{SF_6}}{M_{SF_6}} + \frac{1 - Y_{SF_6}}{M_{air}} \tag{3.5}$$

where t is the time, ρ is the density of the mixture, U is the mean component of the velocity vector, $P' = P + 2/3\rho k$ is the "modified" mean pressure, μ and μ_t are the dynamic and eddy viscosities, g is the gravitational acceleration vector, Y_{SF_6} is the mean value of the SF_6 mass fraction, Γ is the molecular diffusivity of the SF_6, σ_t is the turbulence Schmidt number; M, M_{SF6} and M_{air} are the molar masses of the gaseous mixture, the SF_6 and the air, respectively, T is the temperature of the mixture (20 °C), r is the ideal gas constant, $C_\mu = 0.09$, k is the turbulence kinetic energy and ε is its dissipation rate.

The turbulence viscosity is calculated using the following expression:

$$\mu_t = C_\mu \rho \frac{k^2}{\varepsilon} \tag{3.6}$$

where k and ε are governed by the transport equations:

$$\frac{\partial (\rho k)}{\partial t} + \nabla \cdot (\rho U k) = \nabla \cdot \left(\left(\mu + \frac{\mu_t}{\sigma_k}\right)\nabla k\right) + P_k + G_k - \rho\varepsilon \tag{3.7}$$

$$\frac{\partial (\rho \varepsilon)}{\partial t} + \nabla \cdot (\rho U \varepsilon) = \nabla \cdot \left(\left(\mu + \frac{\mu_t}{\sigma_\varepsilon}\right)\nabla \varepsilon\right) + \frac{\varepsilon}{k}\left[C_{\varepsilon_1}\left(P_k + C_{\varepsilon_3}\max(0, G_k)\right) - C_{\varepsilon_2}\rho\varepsilon\right] \tag{3.8}$$

In these two above equations,

$$P_k = \mu_t \nabla U \cdot (\nabla U + (\nabla U)^{\mathrm{Tr}}) - \frac{2}{3}\nabla \cdot U(3\mu_t \nabla \cdot U + \rho k) \tag{3.9}$$

is the term for the production of turbulence kinetic energy due to mean velocity gradients, and

$$G_k = -\frac{\mu_t}{\sigma_t} g \cdot \frac{\nabla \rho}{\rho} \tag{3.10}$$

is the term for the production of kinetic energy linked to density variations. The latter is taken into account in the Eq. (3.8) only when it is positive (stable conditions).

It should be underlined that the last term G_k is not implemented in CFX version 5.5.1. Nevertheless, a computation performed later with version 5.7.1, which takes account of this term, showed that it had very little influence, as shown in Fig. 5. Indeed, in this study, the scalar product $g \cdot \nabla\rho/\rho$ is always positive, so G_k is only involved in the k transport Eq. (3.7). Moreover, the density gradients are quite low in the room: the density decreases very quickly downstream the injection outlet, and is less than 1.5 kg/m^3 outside the gas jet.

It should be also noted that one of the known drawbacks of the k–ε model is that it does not take account of any anisotropy

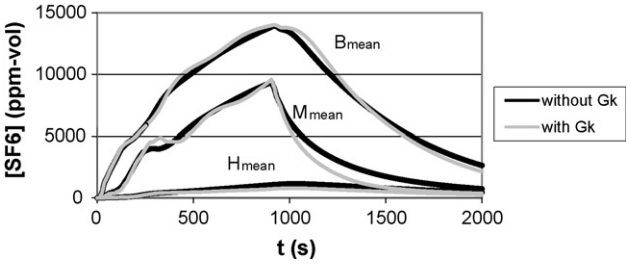

Fig. 5. Influence of the buoyancy production term G_k on the space–time evolution of concentration (test 8).

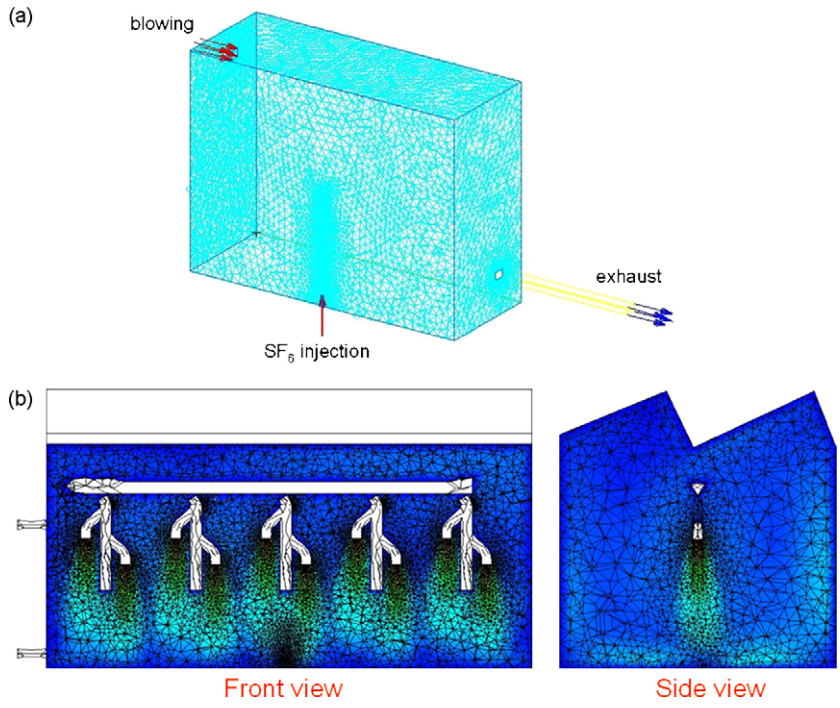

Fig. 6. Geometry and mesh chosen for the 36 m^3 room (a) and the 1500 m^3 room (b).

in turbulent diffusion because the modelling of turbulence correlations is based on the notion of Eddy viscosity μ_t, which does not depend on the direction considered at each point. But, as Pereira and Chen [7], in particular, point out in a study of heavy gas dispersion in the environment, there can sometimes be great anisotropy associated with turbulence in stratified airflows. The authors define an "anisotropic" turbulence viscosity. Here, anisotropy has not been taken into account, as the k–ε model in CFX uses isotropic turbulence viscosity in accordance with the standard model.

3.3. Computation domains

Fig. 6 shows the geometry and mesh used to model the two rooms studied. With the 36 m^3 room, the computation domain only represents half the geometry because of symmetry. The first plane visible in Fig. 6a is therefore a plane of symmetry passing through the centre of the room (and consequently through the injection nozzle). The 1500 m^3 room is represented in its entirety (Fig. 6b). In particular it includes the blowing system; the inlet conditions were applied at the ten blowing openings in operation (two per blowing module).

Mesh refinement was applied downstream of the blowing nozzles and SF_6 injection nozzles. It should be noted that an advanced mesh sensitivity study was carried out, particularly for the 36 m^3 room (see Section 3.4). As regards boundary conditions, Dirichlet conditions were applied to the blowing: a uniform velocity profile was set and the turbulent quantities k and ε were calculated automatically by CFX from the turbulence intensity I (set at the default value 3.7%), the inlet velocity u_{in} and the hydraulic diameter of the vents D_h: $k = 3/2I^2(u_{in})^2$ and $\varepsilon = k^{3/2}/(0.3D_h)$. These expressions, applicable where the inlet is small compared with the size of the computation domain, are well suited to this particular case. Finally, Neumann conditions (free outlet) and atmospheric pressure were applied to exhaust.

3.4. Sensitivity analyses

Many sensitivity studies have been conducted both on the numerical (mesh, time step, number of iterations per time step, etc.) and the physical parameters (turbulence model, etc.). Furthermore, convergence difficulties in the form of high residuals values and large oscillations in the balance of each variable were highlighted during the gas injection phase, due to the very low characteristic times of the injection nozzle emission compared with the characteristic airflow times. These difficulties were resolved using a parameter known as the "local timescale factor", which allows a false local time step to be introduced into each mesh.

The sensitivity studies conducted, mainly on the basis of test 5 (2 min injection) and test 8 (15 min injection), made it possible to identify optimum values for the convergence parameters. Fig. 7 shows the influence of time step during the injection phase of test 8. Discrepancies on results are, as expected, all the largest that the time step value is high, and convergence errors appear from a value of 4 s. From this study, the time step was set to 1 s (this value was confirmed as optimum on other tests). Other sensitivity studies showed that the optimum values for the number of iterations per time step and for the local timescale factor were, respectively, 3 and 10.

As regards the mesh, five grids were studied on the basis of test 8 for the 36 m^3 room (see Table 5), from the coarsest (67,000 elements) to the finest (387,000 elements), altering the size of the mesh in the injection zone, the size of the mesh in

Table 5
Characteristics of the meshes used for the sensitivity study in the 36 m^3 room

	Number of elements	Max. cell size outside the jet (m)	Min. cell size inside the jet (m)	Height of the mesh control line along the injection axis (m)	Grid inflation at the walls
Mesh 1	67,000	0.2	–	–	No
Mesh 2	261,000	0.1	0.02	3	No
Mesh 3	276,000	0.1	0.01	1.5	No
Mesh 4	305,000	0.1	0.01	1.5	Yes
Mesh 5	387,000	0.1	0.002	1	No

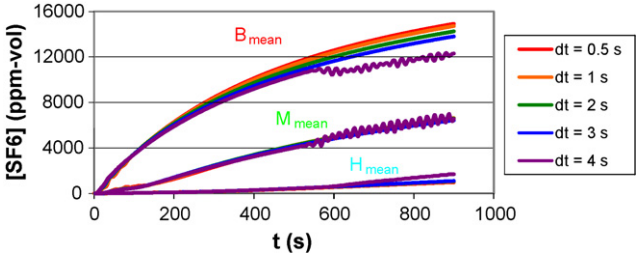

Fig. 7. Influence of the time step on the space–time evolution of concentration (test 8).

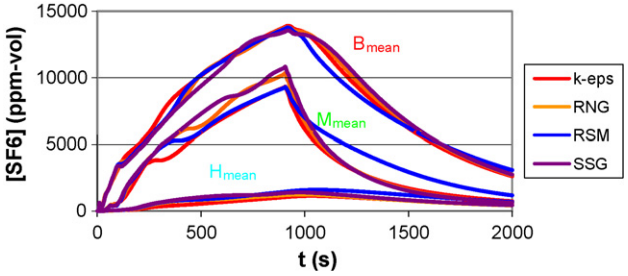

Fig. 9. Influence of the turbulence model on the space–time evolution of concentration (test 8).

the non-injection zone, the extent of the refinement zone and whether or not prismatic meshes were introduced for the walls (a technique known as inflation). On Fig. 8 are compared the results obtained with these five grids during the injection phase of test 8. The grid influence is especially noticeable at the middle points, which are the most influenced by the gas injection and hence by the meshing of the jet region. The grid convergence is almost achieved with mesh 3 (276,000 elements), which has been retained for all the computations performed for the 36 m^3 room. For the 1500 m^3 room, two meshes were studied on the basis of test 17, one of which had 800,000 elements (maximum size of 0.3 m) and the other 348,000 elements (maximum size of 0.8 m); the latter was the one chosen.

The influence of the turbulence model was also studied on the basis of test 8. Four RANS-type models were thus tested:

- the standard k–ε model, chosen as the default,
- the RNG k–ε model, based on renormalisation group analysis of the Navier-Stokes equations; the expressions for k and ε are the same as those for the standard k–ε model; only the constant values differ, and the constant $C\varepsilon_1$ is replaced by a function (strain-dependent correction term),
- the RSM (Reynolds Stress Model) second-order model, in which the turbulence correlations are no longer calculated from a turbulence viscosity but are governed by a transport equation,
- the SSG (Speziale, Sarkar, Gatski) model, which is a variant of the RSM model and which uses a quadratic equation for the pressure–strain correlation term (the latter ensures the redistribution of the kinetic energy among the Reynolds normal stresses).

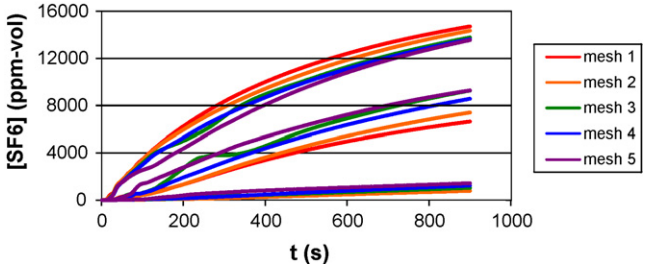

Fig. 8. Influence of the mesh on the space–time evolution of concentration (test 8).

More details about these turbulence models used in the main CFD codes can be obtained in [3–5]. Fig. 9 presents the time evolution of concentration calculated with the different models. Some discrepancies can be observed, especially at the middle monitoring points, as previously noted for grid sensitivity. In particular, the concentration decay predicted by the RSM model after the end of injection is slower than the one predicted by the other models. Nevertheless, overall the differences are minimal, and in all cases the rapid concentration decrease observed experimentally at the middle points are not reproduced by the code (see Section 4.3.3). Hence, in view of these results, the k–ε model, which is the most used in industrial applications and in particular in indoor airflow simulation, was retained for all the simulations.

4. Main simulation results and comparison with the experimental results

4.1. Typical evolution of gas stratification over time

As an illustration, Fig. 10 shows the SF_6 mass fraction fields for test 8, on the symmetry plane passing through the injection pipe (middle vertical plane), obtained at different times during

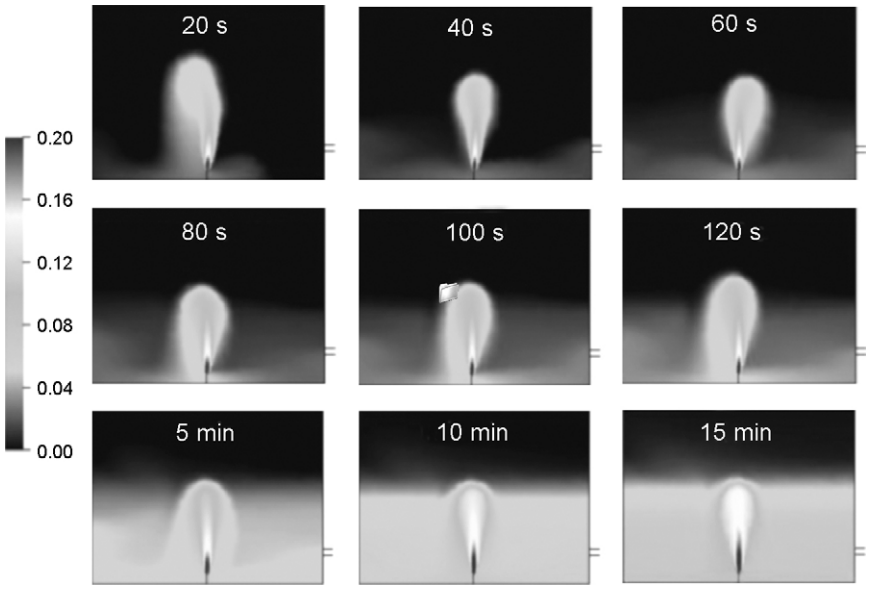

Fig. 10. SF_6 mass fraction fields in the symmetry plane, at different times during the injection phase of test 8.

injection. The jet formed is typical for an ascending heavy gas being injected upwards: it reaches a maximum height and has a rounded tip. For the first minute, the jet is slightly disturbed by the room ventilation, but then it stabilises as the mass fractions become stratified in the room. Because of its density, SF_6 accumulates in the lower part of the room, forming a zone with a relatively high concentration of gas (mass fraction of the order of 10% by the end of injection), the volume of which gradually increases.

4.2. Overall validation of the simulation results

Fig. 11 shows the SF_6 mass fraction field obtained in the middle vertical plane of each room, at the end of gas injection, for each of the tests performed (for the 36 m^3 room, only the results of the simulations performed with continuous ventilation are shown). Stratification can be seen in most cases, due to the accumulation of the SF_6 gas in the lower part of the room. Furthermore, in the 36 m^3 room, injection is observed to have a very strong influence, leading to wide diversity in the configurations studied. Conversely, in the 1500 m^3 room, the results obtained for stratification are similar overall, because the characteristic parameter values for gas injection are very close (the tests differ mainly because of the air exchange rate value).

A first validation of these results was performed by comparing the maximum height of the jet obtained by the code at the end of injection, with the height resulting from the Baines et al. correlation [10]: $X = 1.74 D_{inj}\sqrt{Fr}$ where X (m) is the range of the jet, D_{inj} (m) the diameter of the injection nozzle and Fr the Froude number of the jet, defined by:

$$Fr = \frac{\rho_{inj} V_{inj}^2}{g D_{inj}(\rho_a - \rho_{inj})}$$

where ρ_{inj} is the density of the fluid on injection (SF_6 in this case), V_{inj} the injection velocity, D_{inj} the injection diameter, g the gravitational acceleration and ρ_a the density of the ambient fluid (the air in this case). It should be remembered that the Froude number expresses the ratio between the force associated with the inertia of the jet and the buoyancy force associated with the differences in density.

Fig. 12 shows that the agreement between the results given by CFX and those given by the Baines correlation is very satisfactory. However, it should be noted that the results of the tests performed with discontinuous ventilation in the 36 m^3 room are not shown in this figure (tests 10–15). Furthermore, the maximum height calculated by CFX in the case of test 3 is not shown either because of the impaction of the jet on the ceiling. Besides, this result is consistent with the value resulting from the Baines correlation ($H/Z = 1$).

A second validation was conducted, comparing for each experimental configuration the maximum concentration value at the low points, obtained by computation with the value obtained experimentally. By way of a remainder, these points were located 0.5 m from the ground in the 36 m^3 room and 2 m from the ground in the 1500 m^3 room. Fig. 13 shows good agreement of the results overall. Furthermore, it should be noted that the concentration levels are lower overall in the 1500 m^3 room than in the 36 m^3 one, though comparison is difficult because of the height difference between the low levels in the two rooms.

4.3. Identification of the parameters with the greatest influence

Although the test grids were not designed for a rigorous parametric study of the results, it was nevertheless possible to study the influence of various parameters.

4.3.1. Tests at a high flow velocity

One of the parameters identified as having a major influence on heavy gas dispersion is the velocity of flows within the room

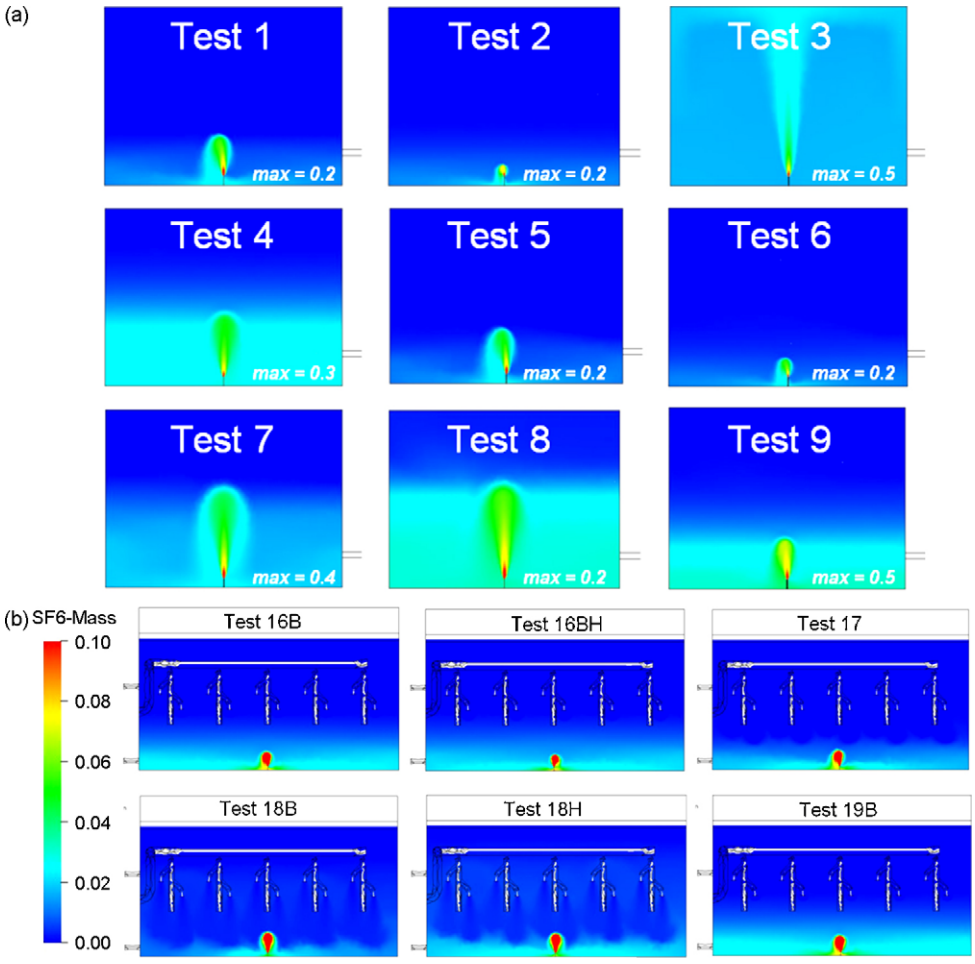

Fig. 11. SF_6 mass fraction field in the median vertical plane of the 36 m^3 room (a) and the 1500 m^3 room (b).

during the gas injection phase, associated with the intensity of flow mixing. Because of the effect of scale, this is driven essentially by the injection of SF_6 into the 36 m^3 room and by the ventilation (air exchange rate or air flow rate from blowing) in the 1500 m^3 room.

As an illustration, Fig. 14 shows a comparison of the computation results with the experimental results for test 3 conducted in the first room. In this test, characterized by the highest Reynolds number at the injection (see Table 1), the range of the jet produced by the injection of SF_6 was very high, contributing to an important flow mixing in the room during the gas injection phase (120 s). A comparison of the time evolution of the concentrations at the low points (red), middle points (green) and high points (blue) during the injection phase proves very satisfactory. Only the phase where the concentration decreases, after injection was stopped, shows differences (this observation is common to all the tests conducted in this room, probably because of the low flow velocities due to the room ventilation when the injection of SF_6 is stopped). In the computation, the decrease is mainly linked to air exchange in the room, while in the experiment, there

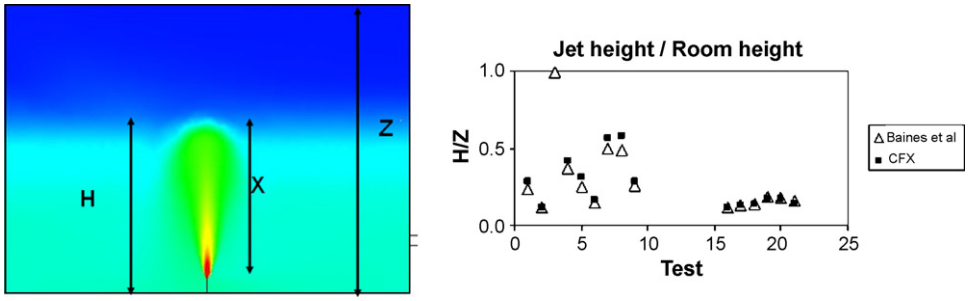

Fig. 12. Comparison of the jet height between CFX and the Baines et al. model.

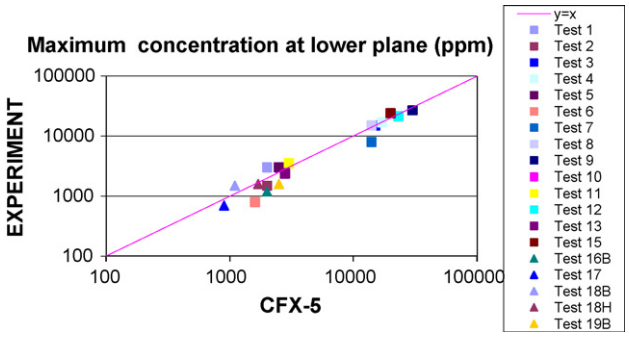

Fig. 13. Comparison of the maximum concentration levels between computation and experiment.

is also an effect linked to the SF_6 falling in the room, firstly at the high level, then at the middle level, and finally at the low level (which adds gas each time to the lower levels). Nevertheless, overall, the concentration levels are well matched by the code.

The comparison in Fig. 15 between the computation results and the experimental results is also satisfactory in the case of tests 18B and 18H, conducted in the second room with the highest air exchange rate. The gas stratification, the concentration levels and the influence of the exhaust position are well matched (increase in the concentration levels, particularly at the high points, when exhaust is high up).

4.3.2. *Tests at a low flow velocity*

The influence of low flow velocities on the evolution of concentrations in the room was previously shown in test 3 by the decrease in concentrations after SF_6 injection had finished. This influence was also apparent during the gas injection phase in tests where there was little flow mixing, i.e. in the tests with a low injection velocity in the first room (tests 2, 6 and 13, characterized by a low Reynolds number at the injection) and the tests with low air exchange rates in the second room (tests 16 and 19). These tests show the largest differences between the simulation results and the experimental results. As Fig. 16 relating to tests 2 and 19B shows very great disparity was revealed experimentally between the different points on the low level, but this disparity was not predicted by the code. In addition, the concentration levels reached at these points were generally overestimated by the code. Finally, it should be underlined that all these experimental tests were characterized by major instabilities and presented reproducibility problems, which confirms the huge influence low velocity has on heavy gas dispersion.

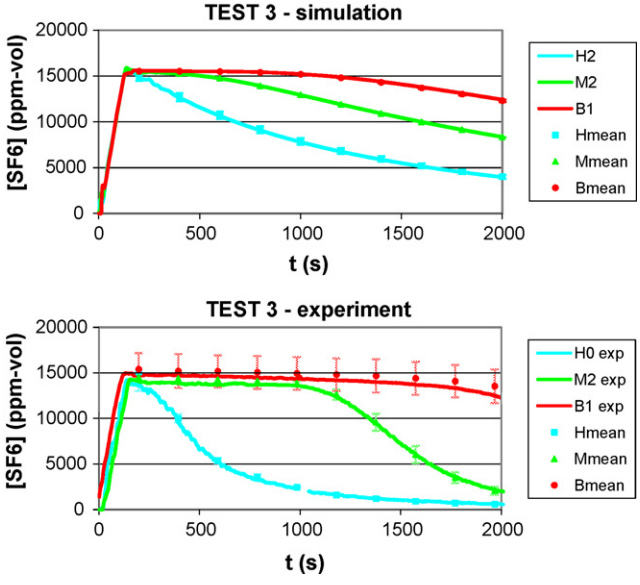

Fig. 14. Test at a high flow velocity in the 36 m^3 room.

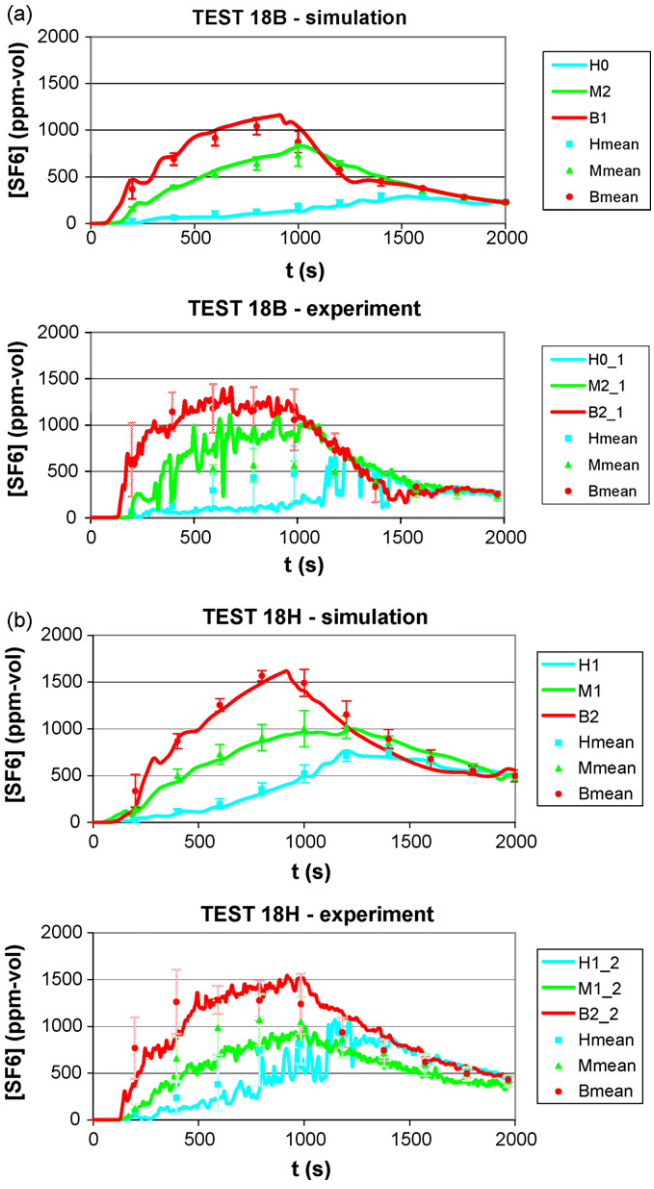

Fig. 15. Tests at a high flow velocity in the 1500 m^3 room (a: low exhaust; b: high exhaust).

4.3.3. *Tests with high concentrations*

Another parameter that seems to have an influence on heavy gas dispersion is the SF_6 concentration level reached in the

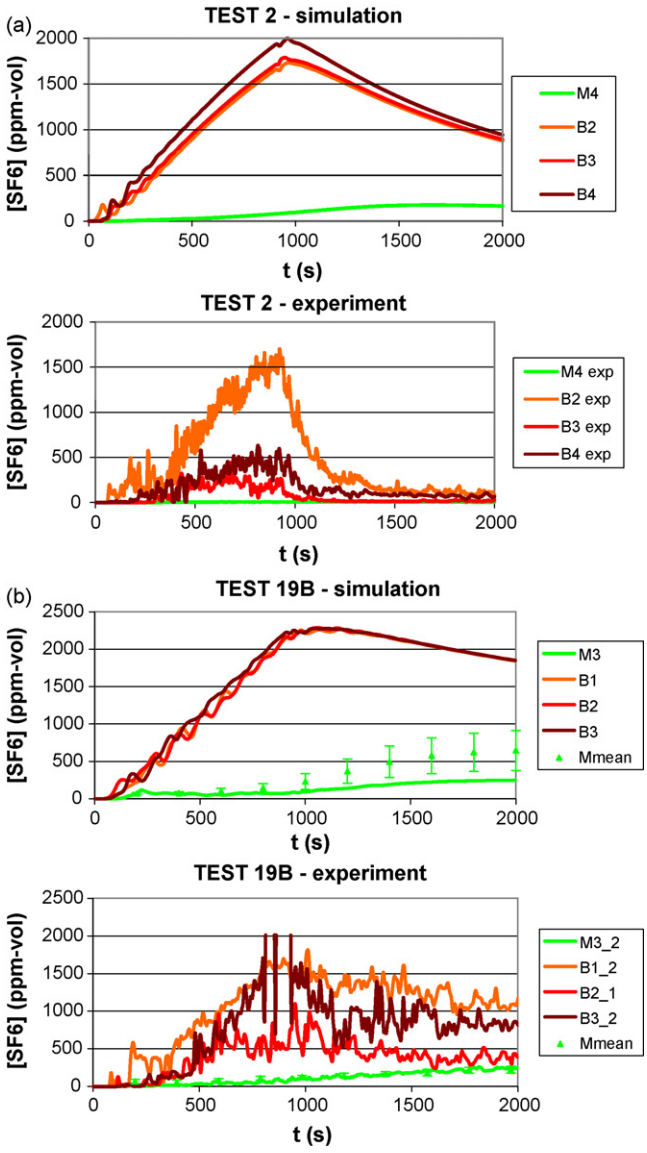

Fig. 16. Tests at a low flow velocity in both rooms (a: 36 m^3 room; b: 1500 m^3 room).

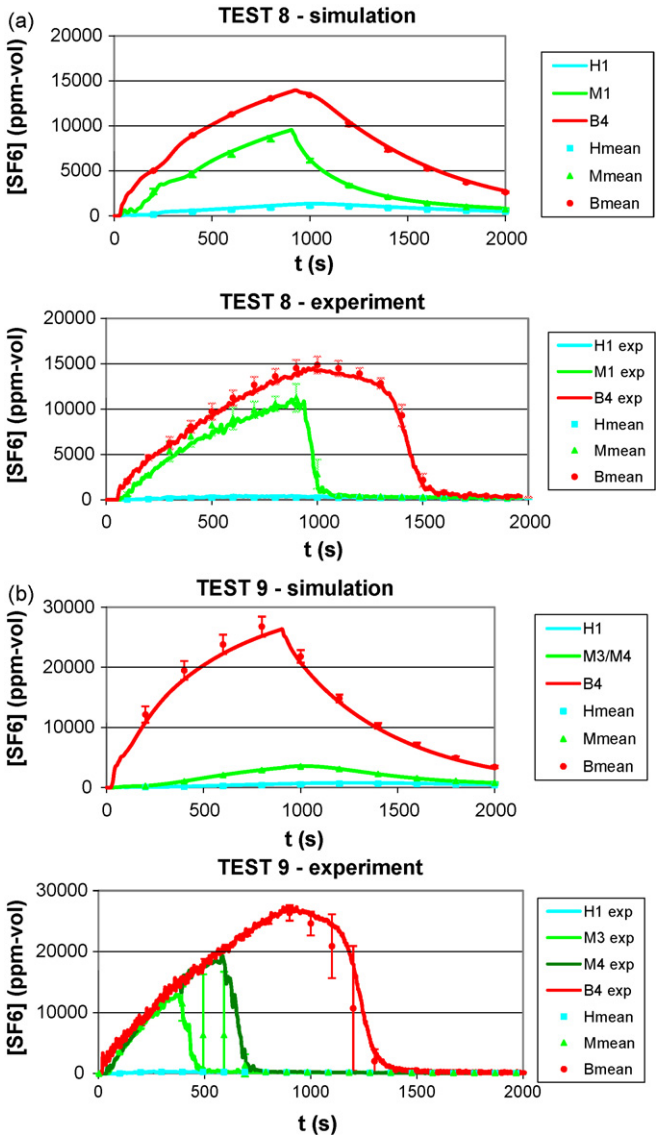

Fig. 17. Tests with a high SF_6 concentration in the 36 m^3 room (a: test 8; b: test 9).

room. During tests 8 and 9 conducted in the 36 m^3 room, where there were high concentration levels of up to 30,000 ppm-vol at the low points (see Fig. 17), a very rapid decrease in the concentrations at the middle points was observed experimentally just after gas injection was stopped (test 8) or even during injection (test 9), demonstrating the instability of the stratification that is established during injection. This behaviour, which was always observed during several reproducibility tests, was not found by the code, which always predicted a relatively slow decrease in the concentrations after injection was stopped, governed essentially by the air exchange rate in the room. Moreover, it should be underlined that the evolutions of concentration at the middle level in test 9, before the rapid decay, are experimentally the same as at the lower level. This atypical result, not reproduced by the code, might be linked to the lowest Froude number at the injection (see Table 1).

5. Conclusion

The experimental study aimed at characterising the effects of SF_6 dispersion demonstrates expected stratification phenomena of concentrations in the different rooms tested, which are accentuated particularly at the lower levels compared with the rest of the room volumes. In addition, it was observed that the gas dispersion was essentially driven by the action of the velocity of the emission jet in the smaller room (36 m^3), while the effect of the room ventilation, added to the effects of the injection jet, was more marked in the larger room (1500 m^3). So the induction phenomena, particularly associated with the increase in the gas injection velocity, favour the gas dispersion effects in the room.

Multidimensional simulations of all the experimental configurations enabled the stratification and the concentration levels reached in the rooms to be predicted overall, and the higher

the flow mixing, the more satisfactory was the comparison between simulation and experiment. However, some differences were revealed; in particular, when gas injection into the rooms stopped, the decrease in SF_6 concentration was linked, in the case of the code, to the air exchange rate in the room, while in the experiments, an additional effect due to the gas falling in the room was observed (thus adding to the lower levels).

In conclusion, this study made it possible to identify some of the parameters that have the greatest influence on the dispersion of a heavy gas in a ventilated room, as well as some expected phenomena (stratification), and some unexpected phenomena (particularly the instability of this stratification). Furthermore, although the qualification of the CFX code can be considered sufficiently satisfactory with regard to the general objectives of the study, limits to this qualification have been clearly highlighted. The subject of high density gaseous pollutant dispersion in a ventilated room consequently requires the performance of additional studies, both from an experimental and a numerical angle. In particular, in terms of modelling, it could be of interest to adopt an LES (Large Eddy Simulation) type approach [11], which could be used to gain a better understanding of the instability phenomena observed, and the change in concentrations where there was a low flow velocity in the room.

References

[1] C. Vavasseur, Application of tracer gas methods to the measurements of ventilation parameters in nuclears plants and various industrial sectors, in: H.D. Goodfellow (Ed.), Ventilation'85, Elsevier, 1986, pp. 785–796.
[2] C. Roussel, A tracer-gas system to evaluate the efficiency of ventilation systems or simulate the consequences of an accident, in: H.D. Goodfellow (Ed.), Ventilation'85, Elsevier, 1986, pp. 291–295.
[3] H.K. Versteeg, W. Malalasekera, An Introduction to Computational Fluid Dynamics – The Finite Volume Method, Longman, New York, 1995.
[4] ANSYS Company, CFX-5 Solver Theory Manual CFX Ltd., Oxfordshire, 2003.
[5] Introduction to the modelling of the turbulence, Lecture Series 2000-04, Von Karman Institute for Fluid Dynamics, 2000.
[6] S. Sklavounos, F. Rigas, Validation of turbulence models in heavy gas dispersion over obstacles, J. Hazard. Mater. A108 (2004) 9–20.
[7] J.C.F. Pereira, X.-Q. Chen, Numerical calculations of unsteady heavy gas dispersion, J. Hazard. Mater. 46 (1996) 253–272.
[8] A. Luketa-Hanlin, R.P. Koopman, D.L. Ermak, On the application of computational fluid dynamics codes for liquefied natural gas dispersion, J. Hazard. Mater. 140 (2007) 504–517.
[9] H.A. Olvera, A.R. Choudhuri, Numerical simulation of hydrogen dispersion in the vicinity of a cubical building in stable stratified atmopsheres, Int. J. Hydrogen Energy 31 (2006) 2356–2369.
[10] W.D. Baines, J.S. Turner, I.H. Campbell, Turbulent fountains in an open chamber, J. Fluid Mechanics 212 (1990) 557–592.
[11] L. Davidson, P.V. Nielsen, C. Topp, Low-Reynolds number effects in ventilated rooms: a numerical study, Roomvent 2000, in: 7th International Conference on Air Distribution in Rooms, vol. 1, 2000, pp. 307–318.